ACS Catalysis

Review

pubs.acs.org/acscatalysis

Tafel Kinetics of Electrocatalytic Reactions: From Experiment to First-Principles

Ya-Hui Fang[†,‡] and Zhi-Pan Liu*[,‡]

[†]School of Chemical and Environmental Engineering, Shanghai Institute of Technology, Shanghai 201418, China

[‡]Shanghai Key Laboratory of Molecular Catalysis and Innovative Materials, Department of Chemistry, Key Laboratory of Computational Physical Science (Ministry of Education), Fudan University, Shanghai 200433, China

ABSTRACT: The Tafel equation is of fundamental importance in electrochemical kinetics, formulating a quantitative relation between the current and the applied electrochemical potential. The recent years have seen the rapid expansion and development in the application of first-principles density functional theory (DFT) simulation on electrocatalytic reactions that occur at the solid−liquid interface. This article reviews the current theoretical methods for electrochemistry modeling, in particular, those for the direct computation of Tafel kinetics of electrocatalytic reactions on surfaces based on DFT calculations. Representative reactions, namely, hydrogen evolution and oxygen evolution reactions, are selected to illustrate how the theoretical methods are applied to compute quantitatively the kinetics of multiple-step electrochemical reactions. We summarize in detail the computation procedure based on the first-principles periodic continuum solvation method for obtaining the charge transfer coefficient (CTC) and deducing the potential-dependent reaction rate. The theoretical results on the Tafel kinetics of electrochemical reactions are generalized and discussed.

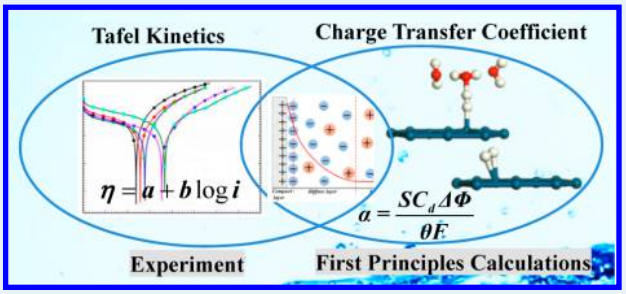

KEYWORDS: *Tafel kinetics, electrocatalytic reactions, charge transfer coefficient, periodic continuum solvation method, first-principles calculations*

1. INTRODUCTION

Electron transfer occurs ubiquitously in nature and is of central importance in chemistry. By establishing the connection between the microscopical chemical reaction with the measurable electric current (i) and external potential (U), electrochemistry provides a unique way to quantify the thermodynamics and kinetics of the reaction and facilitates tremendously an understanding of its physical origin.[1−6] The recent development in first-principles methodology has allowed a quantitative computation of the potential-dependent kinetics at the atomic level, which provides a new predictive tool for understanding and designing reactions at the solid−liquid interface. It is the purpose of this article to review these recent progresses for computing and understanding the activity of electrochemical reactions using first-principles theoretical methods.

The quantitative measurement of potential-dependent kinetics of reaction can be dated back to the seminal work by Swiss chemist, Julius Tafel, who summarized the famous Tafel equation from a large amount of experimental data for hydrogen evolution reaction (HER) on metals.[7] The Tafel equation relates the rate of the reactions, as measured by electric current i, to the applied electrochemical potential, U,[7] via a linear correlation between logi and the overpotential (η), see eq 1. The Tafel equation is nowadays widely utilized in many fields including chemistry,[8−12] materials,[13−15] and even archeology.[16,17]

$$\eta = a + b \log i \quad (\eta = U - U_0) \tag{1}$$

$$b = 2.3RT / \alpha F \tag{2}$$

Tafel plot, logi vs η, is a convenient way to analyze electrode properties and the reaction mechanism.[18−20] From Tafel's early experiment, he already recognized that the parameters a and b in the equation should have fundamental significance since the catalytic performance of metals for HER can be characterized by the value of b.[7] By combining with the Arrhenius equation and Transition State Theory, the Tafel slope b can be derived to be reversely proportional to the so-called charge transfer coefficient (CTC), α in eq 2,[21] where T is temperature and F is Faraday constant. The CTC is an important quantity in electrochemistry, reflecting the nature of electron transfer in elementary reaction.[22−27] While it is commonly assumed that the CTC of elementary reaction is either 0.5 (single electron transfer) or 0 (nonelectron transfer), how to determine exactly the CTC of an elementary reaction in general is a highly challenging question for both experiment and theory.

The past decades have witnessed the application of the Tafel equation to reveal the reaction mechanism and the rate-determining step (rds) of the electrochemical process at the solid−liquid interface.[27−29] However, great uncertainties often

Received: September 2, 2014
Revised: October 23, 2014

   dx.doi.org/10.1021/cs501312v | ACS Catal. 2014, 4, 4364−4376

arise in interpreting the experimental kinetic data, which are related to the empirical parameters intrinsic to the Tafel equation and also the complexity of reactions occurring on the electrode.

It is therefore highly desirable that the complex electrochemical reactions can be computed by modern electronic structure calculation, from which the fundamental understanding can be achieved. Indeed, first-principles density functional theory (DFT) calculations have been utilized to investigate the electrochemical reactions in the past 10 years,[30−34] which were able to provide important information on reaction, such as the energetics and the atomic structures of intermediates. The major concern in simulation is how to describe accurately the electrical double layer at the electrode−electrolyte interface, as classically depicted in Gouy−Chapman−Stern (GCS) model[35−37] shown in Figure 1. Various

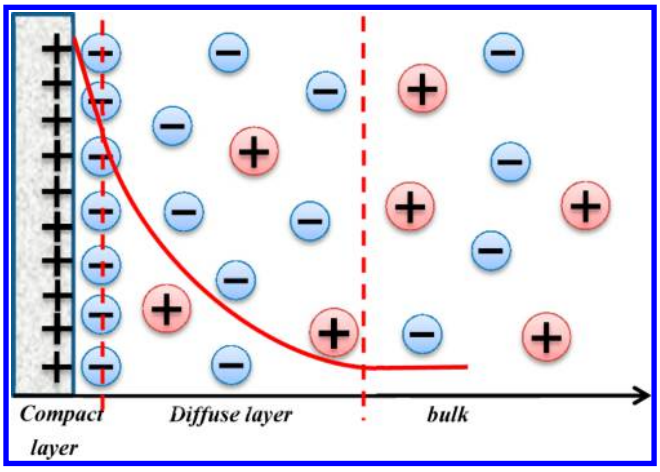

Figure 1. Gouy−Chapman−Stern representation of electrical double layer. The layer closest to the electrode, the *compact layer*, contains solvent molecules and sometimes other species (ions or molecules) that adsorb specifically on electrode. The nonspecifically adsorbed ions are distributed in a three-dimensional region called the *diffuse layer*, which extends from the compact layer into the bulk of the solution.

theoretical approaches have been developed by different groups to simulate the electrochemical reaction, differing in how to treat the water solution, the protons, and charges on the surface.[38−41] The computation of Tafel slope for reaction involving chemical bond making/breaking on electrode has also been attempted,[41,42] which showed that the calculated value is quite sensitive to the solvation (e.g., the configuration of water molecules in the model). Integrating the modified Poisson−Boltzmann-equation-based continuum solvation model with first-principles calculations (DFT/CM-MPB), we recently derive a constant-charge reaction theory to compute the CTC value of elementary electrochemical reactions, which allows us to quantify the effects due to the electrode surface, the solvent, and the chemical bond.[43] Using these theoretical methods, it now becomes possible to resolve the overall potential-dependent reaction kinetics from first principles.[42,44−46]

With the rapid progress in first-principles electrochemistry, a detailed and critical review would be highly necessary to cover this thriving field and motivate further scientific activity. In this article, we mainly focus on the recent development of theoretical methods on computing Tafel kinetics, while the history of Tafel's finding together with the theoretical foundation and the experimental interpretation of Tafel equation will first be overviewed. We will then discuss the application of first-principles Tafel kinetics calculations to two important electrochemical reactions and highlight the comparison between theoretical results and the experimental kinetic data.

2. BRIEF HISTORY OF TAFEL EQUATION AND THEORETICAL FOUNDATION

Since 1895, Tafel investigated the electrocatalytic reduction of organics (e.g., strychnine) for the purpose of synthesizing the organic compounds that are difficult to achieve under typical heat-driven conditions.[47,48] Several metal electrodes (Hg, Pt, Ni, Au, Bi, Cu, and others) were tested in order to improve the cathode performance of organics reduction. It is interesting to find that the HER in water electrolysis is the competitive reaction, especially for the cathode materials with low hydrogen overpotential (e.g., Pt). After years of experiment, Tafel accumulated a large amount data and was able to systematically analyze the HER on different metals. He recognized that a fundamental logarithmic law between overpotential (η) and current (i) is obeyed, which is later termed as the Tafel equation in eq 1.[7] The empirical coefficients a and b can be measured by experiment and a value of b = ∼114 mV was determined for HER on Hg electrode at 26.4 °C in Tafel's original publication in 1905.[7]

Soon after the finding of Tafel, the connection between Tafel equation and the well-known Arrhenius equation in chemical reaction was established. Bulter, Volmer, and their co-workers in 1930s derived electrochemical reaction rate, which can quantitatively rationalize the observed behavior of electrode kinetics with respect to potential,[21] as shown in eq 3, where i_{fd} and i_{rev} are the forward and reverse current density, respectively; i_0 is the exchange current density; R is the gas constant.

$$i = i_{fd} - i_{rev} = i_0 \exp\left(\frac{\alpha\eta F}{RT}\right) - i_0 \exp\left(\frac{-(1-\alpha)\eta F}{RT}\right) \quad (3)$$

At large overpotentials (e.g., above 15 mV) where the electrode reaction becomes irreversible, eq 3 can be simplified to the Tafel equation. The empirical Tafel constants, a and b, can now be derived from eq 4, where the $a = 2.303((RT)/(\alpha F))\log i_0$ and $b = 2.303((RT)/(\alpha F))$ Both constants are related to the CTC α.

$$\eta = -\left(\frac{2.303RT}{\alpha F}\right)\log i_0 + \left(\frac{2.303RT}{\alpha F}\right)\log i \quad (4)$$

The Tafel equation can thus be regarded as a generalized kinetics theory for electron transfer reactions, where the rate of the reaction is related to the overpotential and the apparent CTC α (a composite value linked with different elementary steps). Since most electrochemical reactions involve multiple electron transfer, it can be deduced from microkinetics that the number of electron transferred before the rds should also contribute to the apparent CTC, in addition to the CTC of the elementary rds. For example, if the rds involves one electron transfer with the CTC of 0.5, the overall reaction has the Tafel slopes of $RT/(n + 0.5)F$, where n is the number of electron transfer before rds (n = 0, $2RT/F$ ∼120 mV at 298 K; n = 1, $2RT/3F$∼ 40 mV). On the other hand, if the rds involves zero electron transfer with the CTC of 0, the overall reaction has the Tafel slopes of RT/nF (n = 1, RT/F ∼ 60 mV; n = 2, $RT/2F$ ∼

dx.doi.org/10.1021/cs501312v | ACS Catal. 2014, 4, 4364−4376

30 mV). These "conventional" values have indeed been well observed in experiment, such as in HER on Hg (~114 mV),[7] in OER on RuO_2 (~60 and 120 mV)[49] and in ORR on Pt (~60 and 120 mV),[8] showing the predictive power of the Tafel equation. Generally speaking, some important facts on Tafel slope have been gleaned on the basis of the experimental Tafel kinetics data.

First, the values of Tafel slope $\boldsymbol{b}$ may well not be the classical values as predicted from eq 2, for example, 120 or 60 mV with half-integer or integer apparent CTC. The measured Tafel slope is an apparent value in multiple-step electrocatalytic reactions, which requires the knowledge on the reaction mechanism for further interpreting the kinetics data. For some systems, the measured Tafel slope can be rather scatted due to different experimental conditions. For example, the reported Tafel slope for hydrogen oxidation reaction (HOR) on Pt(111) ranges from 30 to 74 mV, and on Pt(100), it is from 30 to 112 mV.[50,51] The Tafel slope for methanol oxidation (MOR) on Pt ranges from 95 to 440 mV from different experimental groups.[52−54] These experimental results indicate a complex nature of electrocatalytic reactions on electrode: the factors such as the solvent environment and the presence of surface defects may strongly affect the Tafel kinetics.

Second, the Tafel slope is potential-dependent and the abrupt change of Tafel slope at certain potential has been observed in electrocatalytic reactions. For example, the Tafel slope of oxygen evolution (OER) on RuO_2 and oxygen reduction (ORR) on Pt switches from ~120 mV at high $\boldsymbol{\eta}$ to 60 mV at low $\boldsymbol{\eta}$.[8,27,49] The switch of Tafel slope is often regarded as an indication of the change of reaction mechanism (e.g., rds) owing to the change of reaction conditions, including the intermediate coverage and surface morphology induced by the electrical potential.

The ability of the Tafel plot to resolve the mechanism of electrochemistry reaction is therefore needed to assume the values of CTC for elementary reactions (i.e., being zero or 0.5). The validity of the assumption can often be visualized from a 1D potential energy surface (PES) crossing model involving one electron transfer, as described in Marcus theory for the *outer-sphere reaction* (Figure 2), where the reactant (O, oxidant) and the product (R, reductant) do not interact directly with the electrode surface. The definition of CTC $\boldsymbol{\alpha}$ from Marcus theory is the coordinate at the transition state (TS), $q^{\ddagger}$ in Figure 2, along the conceived reaction coordinate for electron transfer. It is thus often called as the symmetry factor $\boldsymbol{\beta}$ computable from the free energy profile[21] in eq 5, where the V refers to the free energy PES. Using the simplest quadratic PES crossing model, the CTC and free energy $\Delta G_f^{\ddagger}$ at TS can be derived as eq 6, 7, where the parameter λ is known as the reorganization energy, the energy required to transform the nuclear configurations of the reactant, including the nearby solvent, to those of the product. The CTC $\boldsymbol{\alpha}$ is a function of both η and λ as expressed in eq 7, showing that it is about 0.5 for one electron transfer reaction when $\lambda \gg \eta$.

$$\alpha = \frac{\partial V_O/\partial q_O}{\partial V_O/\partial q_O - \partial V_R/\partial q_R} \tag{5}$$

$$\Delta G_f^{\ddagger} = \frac{\lambda}{4}\left(1 + \frac{F\eta}{\lambda}\right)^2 \tag{6}$$

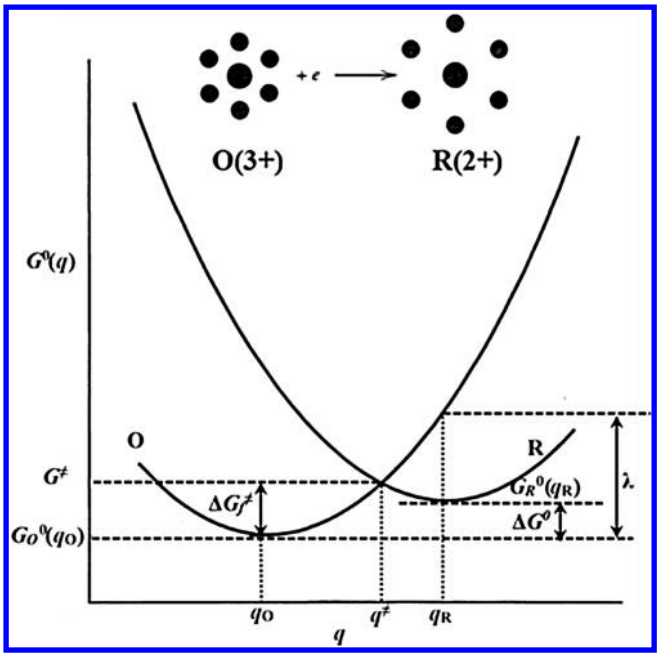

Figure 2. One-dimensional PES profile for standard free energy G^0 as a function of reaction coordinate, q, in one electron transfer reaction (also see the text for the symbols). The inset is a general representation of structural changes (represented by the black dots) that might accompany electron transfer. Figure reproduced with permission from ref 21. Copyright 2001 John Wiley & Sons, Inc.

$$\alpha = \frac{1}{2}\left(1 + \frac{F\eta}{\lambda}\right) \tag{7}$$

The potential dependence of CTC has been tested in experiment to compare with the theoretical prediction. For example, in the reduction reaction of Cr(III) complex (e.g., $Cr(OH_2)_5OSO_3^+$) at mercury electrode in 0.04 M $La(ClO_4)_3$, the measured CTC is ~0.5 at a large potential range (600−1250 mV),[55] and the value for λ/F is estimated to be 2.3 V. In the reduction of organic reduction (e.g., Nitro compounds in aprotic media),[56] the reported CTC values of about 0.4−0.5 at the overpotential range from −500 to 500 mV and the value for λ/F is estimated to be 0.8−1.3 V.

However, the significant deviation of CTC from 0.5 was also observed in the electrochemical reactions occurring on electrodes or involving complex reaction pathways. This is apparently because the electron transfer occurs potentially in a much "smoother" way for reaction on electrode, dictated by the electrode potential and the interactions between the adsorbate and the surface, which is different from the redox reaction in solution where the electron is transferred or is not transferred. Weaver group[57] found that the metal electrodes can exert strong influence on the reaction with hydrated reactants and lead to the unconventional CTC. For $Cr(en)_3^{3+}$ reduction on Pb−Ag electrode,[58] the measured CTC is ~0.8 at −1000 mV vs SCE. In the electroreduction of dialkyl peroxides,[59−61] where electron transfer is coupled with the bond breaking of O−O, the measured CTC is as small as ~0.2, and it shows nonmonotonous dependence with respect to the $\boldsymbol{\eta}$.

Other theoretical models were developed to go beyond the quadratic PES by taking into account the reaction pattern and the environment.[62−66] As pointed out by E.D. German,[67] the CTC $\boldsymbol{\alpha}$ may deviate from 0.5 if the PES of reactant and product, i.e. $\partial V_o/\partial q_o$ and $\partial V_R/\partial q_R$, are modified, as shown in eq

dx.doi.org/10.1021/cs501312v | ACS Catal. 2014, 4, 4364−4376

Table 1. Measured Tafel Slopes for Important Electrocatalytic Reactions

reaction	electrode	solution	b/mV
HER/HOR	Hg	2 M H_2SO_4	116[7]
	Pt(111)	0.5 M H_2SO_4	30[50]
		0.05 M H_2SO_4	74[30]
	Pt(100)	0.5 M H_2SO_4	31[50]
		0.05 M H_2SO_4	112[30]
	Pt(110)	0.5 M H_2SO_4	30[50]
		0.05 M H_2SO_4	28[30]
OER	Pt	1 M $HClO_4$	110[27]
		1 M KOH	59 at low η (η<~400)
			118 at high η (η>~400)[27]
	RuO_2	0.5 M H_2SO_4	59 at low η(η<~300)
			118 at high η(η<~300)[49]
ORR	Pt	0.1 M $HClO_4$	120 at low η(η<~380)
			60 at high η(η>~380)[8]
MOR	Pt	0.5 ML H_2SO_4	95(Pt(553)) and 110(Pt(554)[52]
		0.1 M H_2SO_4	140[53]
		0.1 M $HClO_4$	130;[53] 440[54]
FAOR	Pd	0.5 M H_2SO_4	170[74]

5. Saveant[68] revised the PES using a Morse potential curve to describe the kinetics of electron transfer coupled bond breaking reactions. The contributions of both the chemical bond energy D and solvent reorganization λ need to be included for the computation of CTC, as shown in eq 8. Tsirlina group suggested an additional nonparabolic potential for the strong intramolecular reorganization, and utilized the model to simulate the polarization curve of the $S_2O_8^{2-}$ reduction.[69] More detailed reviews on this topic can be found in ref.[5,63,64,70]

$$\alpha = \frac{1}{2}\left(1 + \frac{F\eta}{D + \lambda}\right) \quad (8)$$

For the reactions occurring on electrodes involving chemical bond making/breaking, it is generally not possible to construct a simple but realistic reaction PES due to the many-body nature of the electrode-molecule coupling. By using the model Hamiltonian approach, the Schmickler group[22,71−73] has computed the CTC of electron and ion transfer reactions on metal electrode. They showed that the CTC value may deviate from the Marcus value of 0.5 due to the symmetry breaking of the TS. The metal *d*-band, solvent, and bond coordinate can all influence the value of CTC. However, due to the many empirical parameters required in the model Hamiltonian approach, the computation of the CTC in general using the model Hamiltonian approach remains infeasible.

3. RESOLVING REACTION MECHANISM BASED ON TAFEL EQUATION AND MICROKINETICS

It is a common practice in electrochemistry to understand the reaction mechanism of electrocatalytic reactions by comparing the theoretically allowed CTC values with the experimental measured ones. The theoretical analyses are based on the Tafel equation and microkinetics. Here we summarize the measured Tafel slope for some important electrocatalytic reactions in Table 1, including HOR, HER, OER, ORR, MOR, and formic acid oxidation (FAOR), and we briefly overview the general procedure of Tafel kinetic analyses in understanding these reactions. Indeed, these Tafel kinetic analyses could provide first insights into the reaction mechanism, but there are obvious deficiencies to produce a self-consistent, atomic-level picture for the electrocatalytic reactions.

HER/HOR. As a prototypical reaction in electrochemistry, HER on metal electrodes (HOR is the reverse reaction of HER) has been extensively studied, and the mechanism is generally regarded to consist of three types elementary reactions.[75] The Volmer (Vol) step (Vol: M + H^+ + e^-↔ $MH_{ads;}$ M is metal electrode) is the initiating step of HER, which is followed either by the H−H bond formation steps via the direct Tafel (Taf) coupling (Taf: $2MH_{ads}$↔ H_2+M), or the Heyrovsky (Hey) step via the proton-coupled electron transfer bond formation (MH_{ads} + H^+ + e^-↔ H_2 + M, Hey). By assuming the CTC value being 0.5, 0, and 0.5 for the Volmer, Tafel, and Heyrovsky step from the reaction formula, respectively, the theoretical Tafel slope can be derived to be 120 ($2RT/F$) mV if the rds is the Volmer step. The theory can thus explain the observed 116 mV Tafel slope for HER on mercury, which is reasonable since the binding energy of H on mercury is rather weak.

For HER on transition metal surfaces where the binding energy of adsorbed H is not weak, the complexity arises due to the finite coverage (θ) of the active adsorbed H atoms (e.g., the underpotential deposited H), which will influence the calculated Tafel slope. For example, if assuming rds is the Heyrovsky step, the calculated Tafel slopes can either be 40 mV ($2RT/3F$) with one Volmer step preceding the Heyrovskey step (θ *is close to* 0), or be 120 ($2RT/F$) mV via the direct Heyrovsky step involving the existing active H (θ is not zero). For HER/HOR on Pt(110), the experimental observed Tafel slope is 28 mV,[51] which thus appears to support the Volmer−Tafel mechanism.

However, HER kinetics on Pt(111) and Pt(100) cannot be rationalized readily from simple theoretical models since the measured Tafel slope is not conventional values, for example, ~ 70 mV on Pt(111) (Table 1). This indicates a complex nature of the electrochemical reaction on the Pt surfaces. Wang et al.[76] suggested that HOR on Pt electrode might proceed via dual pathways, including both Tafel and Heyrovsky mechanisms and they found that a Tafel−Volmer mechanism at a low H coverage (<0.3 ML) can produce the best fit with the experiment rate around the equilibrium potential. The low H coverage fitted from the modeling is however not supported by experimental observation[77] and first-principles calculations.[78,79]

dx.doi.org/10.1021/cs501312v | *ACS Catal.* 2014, 4, 4364−4376

It should be emphasized that the nonconventional CTC values may in fact be quite common for complex reactions, as represented by the electrocatalytic oxidation of organic molecules on electrodes (see Table 1). The measured Tafel slope for MOR (a four-electron oxidation to CO) on Pt ranges from 95 to 440 mV from different experimental groups[52,53,80] and the Tafel slope of ∼440 mV[80] in the recent experiment is particularly large, corresponding to the CTC value of 0.14 (the rate increases with the increase of the potential). Similarly, HCOOH oxidation (FAOR) on Pd/C, the Tafel slope is 170 mV,[74] indicating α being 0.35. The atomic-level mechanism for the electro-oxidation of organic molecules is often controversial because of the presence of multiple reaction channels.[81,82]

OER. Water electrolysis is one of the most important anodic reactions involved in many applications concerning energy storage/conversion.[83,84] Because the reaction causes the major energy loss, the atomic level mechanism of the electrochemical process has been consistently pursued for years[27,85,86] with the aim to design better catalysts. OER involves many possible reaction intermediates, such as OH, O and OOH, and multiple reaction channels. It has been of great interest to understand how the O−O bond is formed on the catalyst surfaces, for example, via O+O → O_2 (O−O coupling) or via H_2O+O → OOH+H^++e, which is regarded to be the rds of OER. Damjanov et al. have suggested 14 possible routes in order to explain the experimental data (the representative routes are listed in Table 2): the observed Tafel slopes are ∼120 mV for Pt in acid solution[27] (Pt electrode will develop surface oxides at the working potentials of OER, i.e. > 1.23 V at acid solution); ∼60 at low η and ∼120 at high η for both Pt in alkaline solution[27] and for RuO_2 in acid solution[49] (Table 1). It was found that the reaction mechanism and rds cannot be unambiguously assigned merely according to the measured Tafel slope.

With the Tafel slope of 120 mV ($2RT/F$) on Pt in the acid solution, several reaction paths (such as 1, 3, and 4, as shown in Table 2) are likely, by assuming the rds as the first charge transfer step. Similarly, it is difficult to understand the switch of Tafel slope from 60 (RT/F) to 120 mV in these systems (Table 1). It can be seen that the paths 6, 10, and 13 with the second step being the rds can lead to a Tafel slope of ∼60 mV and, but none of the paths in the 14 pathways are able to reproduce the slope of ∼120 mV at high overpotentials. It has been recognized that the surface intermediates, coverage, reaction mechanisms, and rds may all be potential-dependent, and thus, the Tafel equation alone is often not sufficient to interpret the mechanism of complex electrochemical reactions.

4. ELECTROCHEMICAL REACTION KINETICS BASED ON FIRST-PRINCIPLES CALCULATIONS

The predictive power of the traditional electrochemical theories becomes limited for understanding the kinetics of complex electrocatalytic reactions, where the electrochemical environment strongly influences the reaction kinetics. To overcome these difficulties, theoretical methods based on first-principles DFT calculations have been developed in the past decade to take into account explicitly the effect of electrode, solvent, and reaction intermediates.[87−100] These methods have been applied to calculate the reaction barrier and the rate of electrocatalytic reactions and understand the reaction mechanism.

Reaction Center Model.[101−106] The reaction center model method developed by Anderson group in 1999 can be utilized to calculate the electron transfer energies for

Table 2. Possible Mechanisms for OER Reaction and the Associated Tafel Slope ($\partial V/\partial \ln i$), As Proposed by Damjanov et al.[a]

	$\partial V/\partial \ln i$		
	anodic		cathodic
	low η	high η	
(1) "oxide path"			
* + H_2O→OH* + H^+ + e^-	$2RT/F$		$2RT/F$
2OH*→O* + H_2O*	$RT/2F$		∞
2O*→O_2 + 2*	$RT/4F$		∞
(3) "hydrogen peroxide" path			
4* + H_2O→4OH* + 4H^+ + 4e^-	$2RT/F$		$2RT/F$
2OH*→H_2O_2* + *	$RT/2F$		$RT/2F$
H_2O_2* + OH*→OH_2* + O_2H*	$RT/3F$		RT/F
O_2H* + OH*→H_2O* + * + O_2	$RT/3F$		∞
(4) "metal peroxide" path			
4* + 4H_2O→4OH* + 4H^+ + 4e^-	$2RT/F$		$2RT/F$
OH*→O* + H_2O*	$RT/2F$		$RT/2F$
O* + OH*→* + HO_2*	$RT/3F$		RT/F
HO_2* + OH*→O_2 + * + H_2O*	$RT/4F$		∞
(6) "alkaline" path			
* + H_2O→OH* + H^+ + e^-	$2RT/F$		$2RT/3F$
OH* + H_2O→$H_2O_2^{-}$* + H^+	RT/F		RT/F
2$H_2O_2^{-}$*→* + O_2^{2-}* + 2H_2O	$RT/2F$	RT/F	$RT/2F$
O_2^{2-}*→*+ O_2 + 2e^-	$RT/3F$		RT/F
(10) Krasilshchikov path (for Ni electrode)			
* + H_2O→OH* + H^+ + e^-	$2RT/F$		$2RT/3F$
OH*→O^{-}* + H^+	RT/F		RT/F
O^{-}*→O* + e^-	$2RT/3F$	$2RT/F$	$2RT/F$
2O*→O_2 + 2*	$RT/4F$		∞
(13) * + H_2O→OH* + H^+ + e^-	$2RT/F$		$2RT/3F$
OH* + H_2O→O−H−OH^{-}* + H^+	RT/F		RT/F
O−H−OH^{-}*→O−H−OH* + e^-	$2RT/3F$	$2RT/F$	$2RT/F$
O−H−OH*→O* + H_2O	$RT/2F$	RT/F	∞
2O*→* + O_2	$RT/4F$		∞

[a]The symbol * stands for a surface site and thus, for example, O* is a surface bound O species. Table reproduced with permission from ref 27. Copyright 1966 Elsevier.

adsorbates. Based on the definition of the electrochemical potential (with respect to the standard hydrogen electrode (SHE) where the work function is about 4.6 eV. Note that 4.6 eV is a commonly used value in the range of 4.4−4.8 eV[107−109]), the method can calculate the potential U according to the ionization potential (IP) and the electron affinity (EA) of the reaction system as shown in Figure 3a, that is, EA or IP = (4.6 + (U/V)) eV. By perturbing the structure along the reaction coordinate with quantum chemical calculations, it is possible to identify the crossing point of potential where the reaction can occur, namely, the reversible potential. For the hydrogen reaction, the reversible potential for Pt−H + H^+ + e (U) ↔ Pt + H_2 is determined to be −0.55 V (apparently due to the limited Pt cluster size[106]). Furthermore, the reaction barrier, E_a, at the reversible potential can be obtained: for HER it is found to be 0.076 eV (Figure 3b).[38,106] Anderson and Cai[38] have resolved the potential-dependent activation energies for HOR on Pt(100) to predict the Tafel kinetics, and they suggested that HOR on Pt(100) follows the Heyrovsky−Volmer mechanism.

The reaction center model is a major step toward understanding the elementary electrocatalytic reaction kinetics under the electrochemical potential. It was noticed that for the

dx.doi.org/10.1021/cs501312v | ACS Catal. 2014, 4, 4364−4376

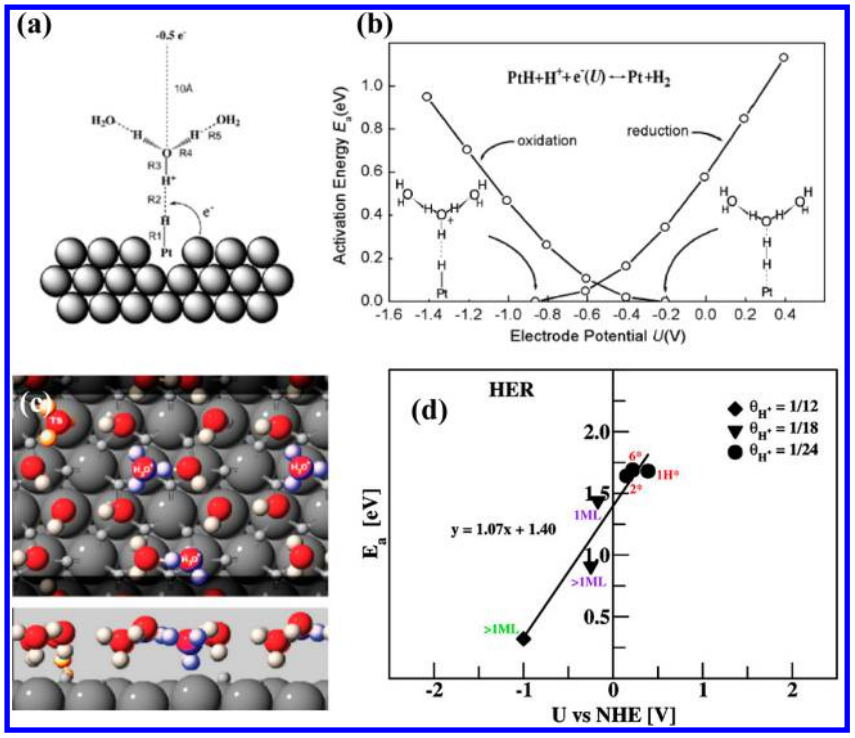

Figure 3. Tafel kinetics calculations of HER on Pt using the reaction center model (a,b) and the periodic slab model (c,d) under the constant charge condition. (a): Scheme of the reaction center model, Pt−H··· $H^+(OH_2)$ $(OH_2)_2$ for HER; (b) Potential-dependent activation energies and the structures of the reduction/oxidation precursors obtained from the reaction center model; (c) Charge-neutral periodic slab model containing solvated protons above Pt(111) surface; (d) Calculated barrier for HER on Pt(111) via Heyrovsky reaction as a function of the electrode potential. Figures reproduced with permission from ref 106 (a,b), Copyright 2004 American Chemical Society; ref 78 (c,d), Copyright 2010 American Chemical Society.

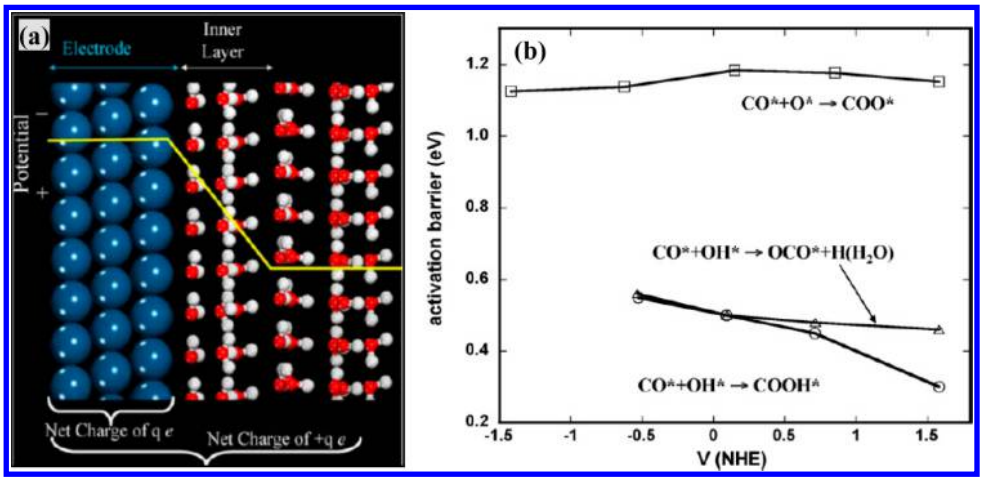

Figure 4. Double-reference method (a) and its application (b) for computing the elementary reaction in CO electrocatalytic oxidation (with O and OH species) on Pt(111). (a): the periodic slab with the vacuum layer filled by static water layers; (b) the calculated barriers against the measured potential from the double reference method. Figures reproduced with permission from ref 112 (a), Copyright 2007 Springer; ref 116 (b), Copyright 2007 Elsevier.

proton-coupled electron reaction (e.g., HER/HOR) the constant charge condition as routinely utilized in quantum mechanics calculation often leads to the varied potentials at the IS and the FS. It is therefore essential to convert the reactivity calculated at the constant charge condition to that at the constant potential condition, which is considered in the experiment. The limitation of the approach is that the metal electrode is only modeled by one or two atoms, which is obviously not realistic for addressing the effects of surface structure and composition.

Instead of searching for the reversible potential point in the reaction center model, the Norskov group proposed an extrapolation scheme in periodic slab calculations to cope with the potential change along the reaction path at the constant charge calculations[40,78] and utilized this scheme to investigate the HER on Pt(111) and Pt(100). In their method, where the water above the surface is modeled using a static bilayer structure, the concentration of H_3O (proton and electron) in the water double layer is altered to mimic the different potential condition (Figure 3c), and the reaction

dx.doi.org/10.1021/cs501312v | ACS Catal. 2014, 4, 4364−4376

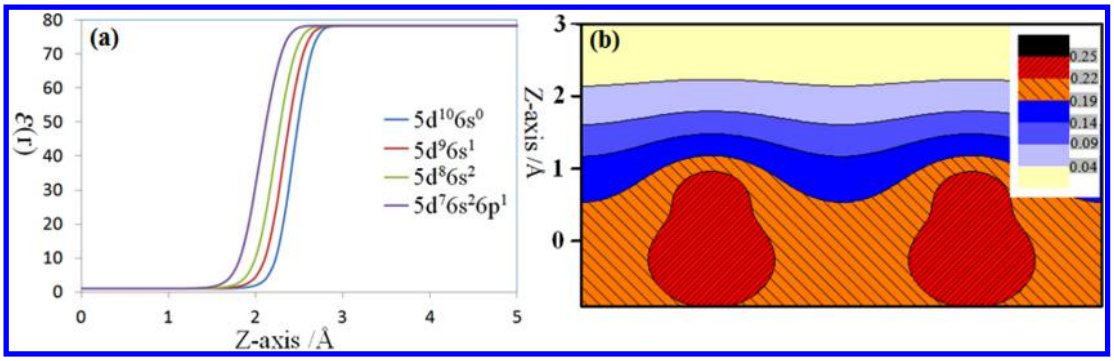

Figure 5. First-principles periodic continuum solvation model based on MPB equation, DFT/CM-MPB method (a) Dielectric function $\varepsilon(r)$ profile as a function of the *z*-axis of the supercell, which can be tuned by modifying the atomic configuration of the element; (b) Contour plot for the change of the total electrostatic potential (ESP) induced by solvation, constructed by subtracting the ESP of a nonsolvated surface from that of a solvated system using CM-MPB. The position of the surface plane is set as zero in *z*-axis (normal to surface plane). Figures reproduced with permission from 44. Copyright 2013 Elsevier.

barriers at each H_3O concentration need to be calculated at several different unit cell sizes. For each unit cell size, the calculated ΔU, the potential difference between two concerned states (e.g., IS, TS, or FS) are recorded, based on which the reaction energy and the reaction barrier can be extrapolated to the zero ΔU limit. They showed that the barrier of HER on Pt(111), including the Heyrovskey and Volmer reactions, decreases with the increase of the overpotential, as shown in Figure 3d. They also found that HERs on both Pt(111) and Pt(100) surfaces prefer the Tafel mechanism, and the calculated barriers on the two surfaces are similar, ∼0.85 eV at the equilibrium potential.[78]

Double Reference Method. In 2006, Neurock and co-workers proposed a double reference method to describe the electrochemical condition, as depicted in Figure 4.[39,110−115] In the method, the electrode surface is represented by the periodic slab model, and the vacuum between slabs is filled with several layers of static water molecules (ice structure). The metal-water interface can be further polarized by altering the number of electrons in the simulation cell and the overall charge neutrality is maintained with a homogeneous countercharge background.

The electrode potential of a given system can be measured by using the double reference method. First, the potential of uncharged system is determined by referring to the vacuum potential (Φ_{vac}), which is obtained by inserting a vacuum layer in the center of the unit cell. Next, the potential at the center of the water layer, being the vacuum potential at the charge neutral condition, is assumed to be constant when the system is charged, and it is taken as the second reference. By this way, the potential of any charged electrode can be "double-reference" to the vacuum potential. For the charged system, the total energy must be corrected by subtracting the unphysical interaction due to the background neutralizing charge, as shown in eq 9 (also see ref 115 on the influence of the thickness of slab in calculations), where $\langle\phi\rangle$ is the volume-averaged electrostatic potential of the cell and Q represents the integration variable.

$$E_{correction} = \int_0^{q_e} \langle\phi\rangle \mathrm{d}Q \tag{9}$$

The double reference method has been utilized to calculate the phase diagram (thermodynamics) of metal surfaces interacting with H_2O solution.[39,111,117,118] It shows that water is activated to form adsorbed hydroxyl, oxygen, and finally a surface oxide layer with the increase of potential. In addition, the barriers of elementary reactions can also be computed by explicitly locating the TS of the catalytic reactions. As shown in Figure 5b, for example, the reaction barrier of the CO + O reaction is shown to be relatively constant at a large potential window, −1.5−1.5 V, but the CO + OH reaction barrier decreases slightly with the increase of potential.[116]

One major concern in the original double reference method is the unrealistic ice-like structure of water layers above the surface, which should be dynamic at ambient conditions and influenced by the potential. Ishikawa and co-workers, using first-principles molecular dynamic (MD), investigated the HOR on Pt_{38} cluster by including 22 waters.[41] To control the effective electrode potential, the Pt cluster was charged by adding/removing a given number of electrons to/from the system, in a manner similar to that discussed in the double reference method. The MD shows that the HOR follows the Tafel−Volmer mechanism (a hemolytic H−H bond cleavage), involving the formation of adsorbed H at the atop site of the topmost Pt and its consequent oxidation into a proton (rds). The calculated barriers are very low, below 3.0 kcal/mol at the reversible potential. Potential-dependent barriers computed for the reaction were then employed to predict a Tafel slope of 30 mV, which is similar to that found on Pt(110) in experiment (Table 1).

Periodic Continuum Solvation Model. To avoid the long-time MD simulation on the structure of the solid−water interface, several research groups have developed independently the periodic continuum solvation model based on the modified Poisson−Boltzmann equation[99,100,119−121] (eq 10), namely, the DFT/CM-MPB method, which can take into account the long-range electrostatic interaction due to the solvation of electrolyte[33,42,44,45] (ν is a parameter relating to electrolyte, $\nu = 2a^3c_b$, a is the effective ion size and c_b is the bulk concentration of the electrolyte). The critical quantity in the MPB equation is the distribution of the dielectric function $\varepsilon(r)$ at the solid−liquid interface.

$$\nabla\cdot(\varepsilon(r)\nabla(\psi)) = -4\pi\rho + 8\pi zec_b\frac{\sinh(ze\psi/kT)}{1-\nu+\nu\cosh(ze\psi/kT)} \tag{10}$$

$$\varepsilon(\rho(r)) = 1 + \frac{\varepsilon_\infty - 1}{2}\left[1 + \frac{1-(\rho(r)/\rho_0)^{2\beta}}{1+(\rho(r)/\rho_0)^{2\beta}}\right] \tag{11}$$

$$U_{cal}^{q} = (\Phi_{ref} - \Phi_F) - 4.6 \tag{12}$$

dx.doi.org/10.1021/cs501312v | ACS Catal. 2014, 4, 4364−4376

Although the detailed implementation might be varied, the essence of the method is to utilize the electronic density from first-principles calculations for solving self-consistently the electrostatic potential of the electrode/electrolyte interface. In the implementation of DFT/CM-MPB method in our group,[122] the continuum dielectric medium is introduced via a parametrized smooth dielectric function $\varepsilon(r)$ (eq 11) as first suggested by Fattebert and Gygi.[123] In the equation, ρ_0 and β are the only two parameters: ρ_0 is the threshold of electron density $\rho(r)$ to adjust the size of the cavity, whereas β determines the smoothness of the transition from 1 to ε_∞. We utilize the soft atomic density determined from pseudopotential for calculating the distribution of $\varepsilon(r)$: for the Pt(111) surface, this is illustrated in Figure 5a, showing the dielectric function increases from 1 (metal bulk) to 78.36 (water solution) within a thickness of ∼3 Å from the surface plane, and the distribution can be further tuned by using different atomic configurations of Pt element.[44]

The DFT/CM-MPB method allows naturally the charged slab calculations. The Boltzmann distribution of the ionic charge (i.e., counter charge) is determined by the second term in the right-hand side of MPB, which can be solved self-consistently during electronic structure loops with the constraint of the total charge conservation. In our implementation, the neutralizing charge in system is distributed following the MPB equation at the grid points of vacuum in the periodic slab calculation. To accommodate the charges in MPB distribution, a large vacuum region along Z axis is often required to separate the adjacent slabs. By this way, the electrochemical potential, i.e. U^q_{cal}, of a system with a net charge q referring to SHE can be calculated by using eq 12, where the computed work function in solution $(\Phi_{ref} - \Phi_F)$ is defined as the potential difference between the Fermi Level Φ_F and the potential level in solution Φ_{ref}

In the framework of DFT/CM-MPB method, the effects due to the solvation and the electrochemical potential (surface charging) can be included straightforwardly and thus allows the computation of the kinetics of complex electrocatalytic reactions, including the proton-coupled electron transfer reaction. Not limited to electrocatalytic reactions, the DFT/CM-MPB methods have also been applied to heterogeneous catalytic reactions at the solid−liquid interface in general, including the photocatalytic reactions.[124,125] The equilibrium properties of double layer of a series of metal electrodes and CO-covered Pt electrode, such as the potential of zero charge and the differential capacitance, have been calculated from theory,[44] and a good agreement between the theoretical values and experimental data has been reported recently. For example, the solvation of metal surface can be visualized by plotting the change of total electrostatic potential on moving from the vacuum to the solution. Figure 5b shows evidently that the Pt surface is strongly polarized by solvation, which places a net positive electrostatic field on the surface and effectively decreases the work function of the surface. In response to the positive electrostatic field, the extra electron will accumulate onto the surface and help to stabilize the surface (reduce surface energy).

Two additional points might be mentioned related to the DFT/CM-MPB method. (i) The accuracy on the solvation energy and potential: The current DFT is problematic for computing accurately the work function in vacuum (see e.g., refs 44, 126) and also the total energy, the MPB method with fitting parameters can help to reduce the absolute error in potential of zero charge and yield solvation energy close to the experimental values, as commonly practiced in quantum chemistry packages. (ii) The necessity of explicit water: The CM-MPB method only takes into account the long-range electrostatic effect due to the solvation. In chemical reactions, where the short-ranged polarization that is of quantum origin is often critical, the explicit water should be taken into account at the reaction center. For computing the electrochemical potential, we found that, however, the presence of explicit water molecules may not be essential since the water−metal interaction is not strong and covered via the parameter fitting.

5. CONSTANT-CHARGE REACTION THEORY FOR POTENTIAL-DEPENDENT REACTION KINETICS USING CM-MPB METHOD

The advent of the DFT/CM-MPB method has allowed the inclusion of the effect of electrode, solvent, and electrolyte in one unified framework. On the basis of the DFT/CM-MPB method, we have developed the constant-charge reaction theory for studying the potential-dependent reaction kinetics at the interface.[42,44−46,127] The constant-charge reaction theory is a practical and general-purpose theoretical tool to establish the quantitative linkage between the Tafel kinetics (current vs potential) and the electrochemical condition, including coverage, surface structure, and the surface charging. In the following, we outline three major steps for applying the method for calculating Tafel kinetics.

Step 1. Determine Surface Phases. For the electrocatalytic reaction at a certain potential condition, it is essential to first know the relevant surface phases and structures.[127,128] In the simplest cases (e.g., planar surfaces without significant restructuring and the coverage of adsorbate being the only concern) one can correlate the surface coverage with the applied potential. Many methods are available for this purpose, that is, computing the thermodynamics in electrochemistry—for example, the Norskov thermodynamics method,[34,40,118] double reference method.[39,118] Here we focus on the DFT/CM-MPB method, where the surface can be explicitly charged to take into account the surface polarization at different potential conditions.

Let's consider an adsorption/desorption redox reaction $A^+ + e^- \leftrightarrow A^*|_\theta$, in which the reaction free energy $\Delta G_{\theta_i}(U)$ of the reaction can be calculated for each θ_i at different potentials U by using the charged-slab DFT/CM-MPB calculations. The relative portion of a phase at U, $x_i(U)$, is obtained using eq 13 from the partition function. The overall coverage at the potential U $(\theta(U))$ can finally be derived by summing up the contributions from all the phases by using eq 14.

$$x_i(U) = \frac{e^{-\Delta G_{\theta_i}(U)/RT}}{\sum_i e^{-\Delta G_{\theta_i}(U)/RT}} \tag{13}$$

$$\theta(U) = \sum_i (\theta_i \times x_i(U)) \tag{14}$$

Step 2. Compute CTC of Elementary Steps. In the constant-charge reaction theory, the constant-potential expression of CTC (eq 15) can be rewritten as the form (eq 16) related to the derivative with respect to the surface free charge (i.e., net charge), the differential capacitance C_d (= $\partial\sigma/\partial U$), and $\boldsymbol{\sigma}$ as the surface charge density (free charge per area). The superscript A and B stand for two states in reaction (e.g., IS, TS, and FS). Both the $\partial G/\partial\sigma$ and C_d terms are quantities that can

dx.doi.org/10.1021/cs501312v | ACS Catal. 2014, 4, 4364−4376

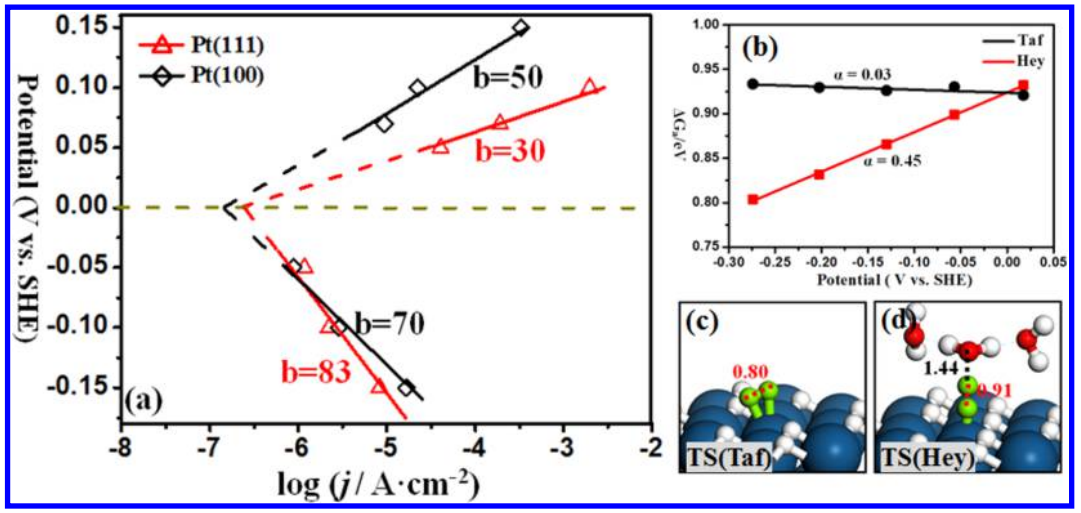

Figure 6. HER/HOR Tafel kinetic from DFT/CM-MPB method. (a) Tafel plot ($U \sim \log(j)$) for HER on Pt(111) and Pt(100); (b) Potential-dependence of the reaction barrier (ΔG_a) for the elementary Tafel and Heyrovsky reaction on 1 ML H/Pt(111). (c) and (d) are the located TSs for Heyrovsky and Tafel step, respectively. Labeled distances are in Angstrom. The produced H_2 molecule at the FS is omitted for clarity. Large Ball: Pt atoms; small red ball: O atoms; small white/green ball: H atoms. Figures reproduced with permission from ref 45. Copyright 2013 American Chemical Society.

be obtained straightforwardly from first-principles calculations. It should be mentioned that eq 16 assumes the constant C_d during the chemical reaction, which is based on the fact that chemical reaction is rare event: when a reaction occurs, the whole surface could be considered as intact with unchanged differential capacitance (this has been illustrated numerically from DFT/CM-MPB calculation[43]). The C_d value can be measured from experiment and thus serves as a benchmark for theoretical calculations.[44,129] In the constant-charge expression, the CTC for reactions at the solid−liquid interface is also derived to be linearly proportional to the electrochemical potential change from the initial state to the transition state as well the interface differential capacitance (C_d) at the constant-charge model (eq 17), where Φ is the absolute electrode potential ($\Delta\Phi$ is thus the difference of Φ between the two states A and B) and S is the unit surface area (e.g., the area of one surface Pt atom on Pt surface). The appearance of the negative value of CTC is likely in eqs 15−17 due to the more convenient definition with respect to the absolute potential instead of overpotential in calculations.

$$\alpha = \frac{\partial \Delta G}{F \Delta U} \tag{15}$$

$$\alpha = \frac{\partial \sigma}{F \partial U}\left(\frac{\partial G_B}{\partial \sigma} - \frac{\partial G_A}{\partial \sigma}\right) \tag{16}$$

$$\alpha = \frac{C_d}{F}\frac{\partial \Delta G_{A\to B}}{\partial \sigma} = \frac{SC_d\Delta\Phi}{\theta F} \tag{17}$$

Step 3. Deduce Tafel Kinetics (Current vs Potential). Using the potential-dependent kinetics data, it is possible to deduce the apparent kinetics according to the microkinetics. The overall current j_{tot} is a function of potential U, which can be calculated by summing up the contribution, j_p, from all the pathways (labeled by subscript p) at the potential U, as written in eq 18. For one particular reaction pathway, the current, j_p, is expressed as the net current of the oxidation (j_O) and reduction (j_R) currents (eq 19), and j_O or j_R can be calculated using the standard rate equation, as eq 20, in which A is the preexpoential factor; S is the total surface area; $[R]$ is the concentration of the reactive site (ML); The apparent free energy barrier $\Delta G_a(U)$ may be simply calculated from eq 21 by summing the contributions from all the possible phases (assuming the active site concentration $[R]$ are the same).

$$j_{tot} = |\sum_p j_p| \tag{18}$$

$$j_p = j_O - j_R \tag{19}$$

$$j_{O/R} = AFS^{-1}N_A^{-1}e^{-\Delta G_a(U)/RT}[R] \tag{20}$$

$$\Delta G_a(U) = -RT\ln[\sum_i x_i(U)e^{-\Delta G_a(\theta_i,U)/RT}] \tag{21}$$

6. APPLICATIONS OF THE CONSTANT-CHARGE REACTION THEORY

6.1. HER/HOR Reaction. The DFT/CM-MPB method has recently been utilized to resolve the mechanism of HER/HOR on Pt and Au surfaces,[45] as shown in Figure 6. The surface phases of these surfaces were first determined and, not surprisingly, on all the surfaces the H coverage was shown to be dependent on the applied electrochemical potential: by reducing the electrochemical potential, one can gradually build up the coverage of the surface H. The dominant local H coverage on Pt(111) and Pt(100) are 1 and 1.5 ML, respectively, at 0 V vs SHE.

On each coverage condition, the lowest energy reaction pathways were determined, and the reaction barriers (ΔG_a) were then identified. The DFT/CM-MPB results show that the calculated ΔG_a of the Heyrovsky reaction (Figure 6d) decreases linearly with the increase of the potential U, while ΔG_a of Tafel reaction (Figure 6c) is rather constant over the investigated potentials, exemplified by the reaction on 1 ML H/Pt(111) shown in Figure 6b. By fitting linearly the barrier ~ overpotential relation ($\Delta G_a = \Delta G_a^0 - \alpha F\eta; \eta = U$), we deduce the charge transfer coefficient α as 0.45 and 0.03 for the Heyrovsky and Tafel reaction, respectively. These determined α confirms the general assumption in electrochemistry that α is

dx.doi.org/10.1021/cs501312v | ACS Catal. 2014, 4, 4364−4376

~0.5 for an ideal single electron transfer elementary reaction; furthermore, it is zero for the nonelectron transfer reaction.

The overall Tafel kinetics of HER/HOR on Pt(111) and Pt(100) under acidic conditions (pH = 0) have been deduced, as shown in Figure 6a. The theoretical Tafel slopes for HER are determined to be 83 mV on Pt(111) and 70 mV on Pt(100), which are generally associated with the reactions involving the minority weakly adsorbed H, that is, the top H above 1 ML on Pt(111) and the bridging H above 1.5 ML on Pt(100). By extrapolating j_{tot} to the equilibrium potential, j_0, we found that j_0 for the two Pt surfaces is ~10^{-7} A cm^{-2}, but the calculated exchange current density (j_0) is generally lower than that measured in experiment for Pt catalyst (~10^{-4} A cm^{-2}).[51,130] It is suggested that HER at the minority surface steps (e.g., Pt(211)) could have a much higher activity than it at terraces, which is responsible for the overall activity on typical Pt electrodes.

6.2. OER in Water Electrolysis. By determining the surface phase diagram, exploring the possible reaction channels, and computing the Tafel lines, the OER kinetics on a RuO_2(110) from the atomic level has recently been elucidated using the DFT/CM-MPB constant-charge reaction theory, as shown in Figure 7.[42]

It was found that the OER occurs directly on an O-terminated surface phase above 1.58 V vs SHE but indirectly on a OH/O mixed phase below 1.58 V by converting first the OH/O mixed phase to the O-terminated phase locally. The rate-determining step of OER involves an unusual water oxidation reaction following a Eley−Rideal-like mechanism, where a water molecule from solution breaks its OH bond over surface Os with concurrent new O−OH bond formation(Figure 7b). The free energy barrier is 0.74 eV at 1.58 V, and it decreases linearly with the increase of potential above 1.58 V (a slope of 0.56) (Figure 7a inset). In contrast, the traditionally regarded surface oxygen coupling (Figure 7c) reaction with a Langmuir−Hinshelwood mechanism is energetically less favored, and its barrier is also weakly affected by the potential (Figure 7a inset). On the basis of the results, the theoretical Tafel lines (Figure 7a) were calculated with the slope fitted to be 55 and 105 mV for OER below and above 1.58 V, respectively. These data are generally consistent with the experimental, that is, two different Tafel slopes, 59 and 118 mV with the switch occurring at 1.52 V.[49]

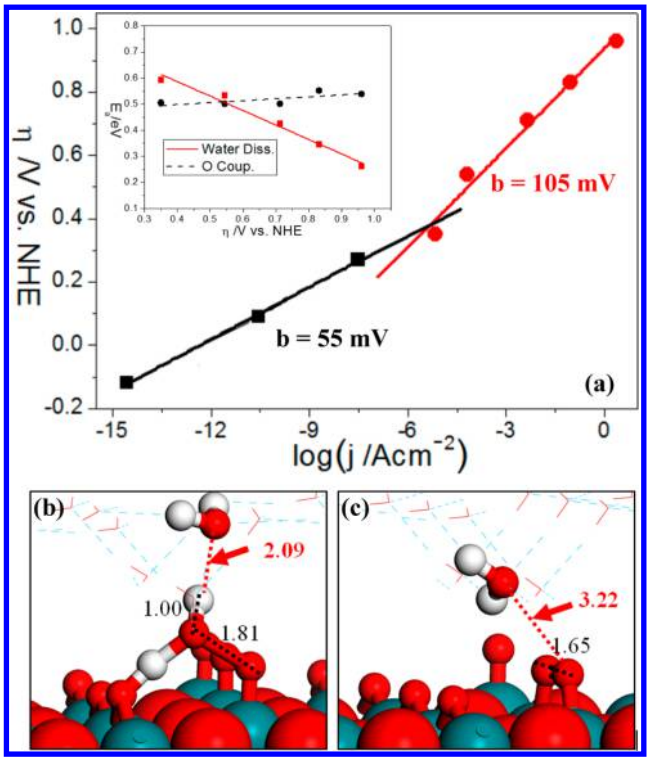

Figure 7. OER kinetics on RuO_2(110) from DFT/CM-MPB method. (a) Plot of reaction barrier E_a against the overpotential η for the water dissociation and the surface oxygen coupling on the O-terminated phase of RuO_2(110). Inset in (a) shows the calculated Tafel lines (log(j) ~ η plot) for OER on RuO_2(110). The slopes, b = $\partial\eta/\partial\log(j)$, of the fitted lines are indicated. (b) and (c) are TS structures of the water dissociation and surface oxygen coupling on the O-terminated phase of RuO_2(110) respectively. All the distances labeled are in Angstrom. O: red ball; H: white ball; Ru: green ball. Figures reproduced with permission from ref 42. Copyright 2010 American Chemical Society.

6.3. Classification of Electrocatalytic Reactions. Using the constant-charge reaction theory, the CTC of typical elementary reactions on metal surface involving the common O−O, C−H, O−H, H−H bond breaking/formation have been computed recently, as shown in Figure 8. According to the CTC values, these reactions can be roughly classified into three classes.

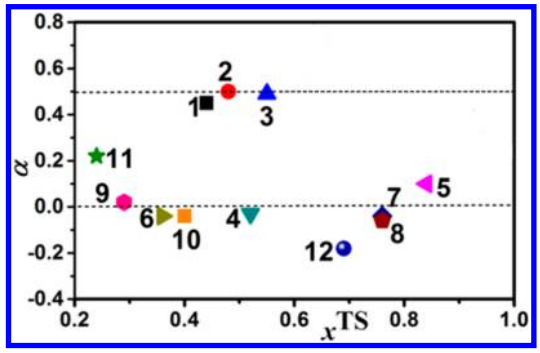

Figure 8. Plot for the computed CTC of the reactions against the reaction coordinate of the TS, x^{TS}. The appearance of the negative value of CTC is due to the more convenient definition with respect to the absolute potential instead of overpotential in calculations. The reaction coordinate of the IS and the FS are defined as 0 and 1 in x-axis, respectively. These reactions are 1: H + H_3O^+(aq)+e→ H_2 + H_2O, 2: O_2 + H_3O^+(aq) + e→ O + OH + H_2O, 3: O + H_3O^+(aq) + e→ OH + H_2O, 4: H + H→ H_2, 5: CO + O → CO_2, 6: CO + OH→ COOH, 7:CH_2OH + H → CH_3OH, 8: CH_3O + H → CH_3OH, 9: O_2 → O + O, 10: CH_3CH_2OH−$(H_2O)_2$ → CH_3CHOH−$(H_2O)_2$ + H, 11:CH_3OH−2$(H_2O)_2$ → CH_3O−2$(H_2O)_2$ + H, 12: CH_3OH−$(H_2O)_2$→ CH_2OH−$(H_2O)_2$ + H. Figure reproduced with permission from ref 43. Copyright 2014 American Chemical Society.

The Class I features with Eley−Rideal type reaction where one reactant in solution reacts with the adsorbate on the surface. In this class of reaction, the electron transfer is coupled strongly with the chemical bond making/breaking with solvated ions directly taking part in reaction. The CTC of these elementary reactions are calculated to be around 0.5. In Figure 8, there are three reactions belong to this class, namely, H + H_3O^+, O_2 + H_3O^+, and O + H_3O^+ reactions, and their CTC are calculated to be 0.46, 0.50 and 0.49, respectively, which agrees with the general assumption in electrochemistry.[27] The Class II features with the Langmuir−Hinshelwood-type reaction where reactants adsorb on the surface to recombine or dissociate. The

dx.doi.org/10.1021/cs501312v | ACS Catal. 2014, 4, 4364−4376

CTC of these elementary reactions is generally close to zero, and the barrier ΔG_a is weakly dependent on potential. Obviously, the electron transfer is decoupled from the chemical bond making/breaking in the Class II reaction. No matter what kind of chemical bond (e.g., H−H, O−O, C−H, O−H, C−O) is involved, the results show that the barriers of these reactions, associative or dissociative, are generally insensitive to the potential, indicating essentially no surface dipole change in the reaction.

Class III are the exception cases, in which the value of α is unconventional, being neither close to ±0.5 nor to zero. In this class of reaction, the coupling between electron transfer and the chemical bond making/breaking is not as obvious as Class I reactions. Shown in Figure 8, two reactions at solid−liquid interface both related to CH_3OH dissociation has been identified, namely, the initial O−H bond breaking with the α of 0.22 and the initial C−H bond breaking with the α of 0.18. The fundamental reason for these unconventional CTC value have attributed to the dramatic structure change of solvation shell from the IS to the TS.[131] The large α indicate that these two reactions might be formally written as, $CH_3OH-(H_2O)_2 \rightarrow CH_3O-(H_2O)_2^{q-} + H + q^+$, and $CH_3OH-(H_2O)_2 \rightarrow CH_2OH-(H_2O)_2^{q+} + H + q^-$, which are consistent with the polarization character of the CH_3O and CH_2OH fragments on metal surface.

7. CONCLUDING REMARKS

Born over a hundred years ago, the Tafel equation continues to be the major tool in electrochemistry for analyzing reaction kinetics and providing insight into the reaction mechanism of electrochemical processes. In the last 10 years, thanks to the rapid progress on the first-principles theoretical methods, the understanding on the kinetics of electrocatalytic reactions at the solid−liquid interface has reached to the unprecedented atomic level, where the quantum mechanics governing electron flow during redox reaction on the solid−liquid interface is coupled with the Newtonian movement of electrode surfaces and electrolyte molecules. The preceding sections serve to highlight some key aspects on the theory of Tafel equation and how the recent theoretical development could help to provide fundamental insights into the Tafel kinetics.

The reaction center model, double reference method, and CM-MPB method are major techniques developed for computing the potential-dependence of chemical reactions. These methods have been utilized for some prototypical reactions on metal and metal oxide surfaces, including HER/HOR, CO oxidation, OER, methanol and formic acid oxidation. The key roles of electrochemical potential on influencing the surface phases, the reaction barriers and kinetics are identified and the quantification of the kinetics from first-principles CM-MPB calculations helps to resolve some of the long-standing puzzles in experiment. Three classes of elementary electrochemical reactions on surfaces are outlined, which laid the fundamental basis for understanding the CTC of reactions on surfaces in general.

It is also noticed that because of the complex electrochemical reaction conditions, including electrode surface, the adsorbates, the electrochemical potential (the surface charging), and the electrolyte, all current methods have some merits but also obvious deficiencies. Thus, the current applications are mainly limited to well-defined, nonreconstructed crystalline planes together with pure water solvent, often treated implicitly or as static ice structures. The determination of the absolute electrochemical potential, the investigation for the electrochemical kinetics of defected/restructured surfaces and even nanoparticles, the multiscale kinetics modeling of electrochemical reactions, and the simulation of photoelectrocatalytic reactions are some important examples that are still highly challenging to solve. Considering the rapid progress in experiment, in particular the emergence of new electro-photocatalytic systems with increasing complexity, there is certainly plenty of room for the new design and the improvement of current theoretical methods for better describing the solid−liquid interface and the reaction therein.

AUTHOR INFORMATION

Corresponding Author

*E-mail: zpliu@fudan.edu.cn (Z.-P.L.).

Notes

The authors declare no competing financial interest.

ACKNOWLEDGMENTS

This work is supported by NSFC (21173051, 21361130019, 21103110), 973 program (2011CB808500, 2013CB834603), Science and Technology Commission of Shanghai Municipality (08DZ2270500), Innovation Program of Shanghai Municipal Education Commission (13YZ120), and "Chen Guang" project supported by Shanghai Municipal Education Commission and Shanghai Education Development Foundation, China and Shanghai Postdoctoral Science Foundation (2012M520040, 2013T60413, 12R21411200) for financial support.

REFERENCES

(1) Bonnet, N.; Marzari, N. *Phys. Rev. Lett.* **2013**, *110*, 086104.
(2) Ludlow, M. K.; Soudackov, A. V.; Hammes-Schiffer, S. *J. Am. Chem. Soc.* **2010**, *132*, 1234−1235.
(3) Viswanathan, V.; Norskov, J. K.; Speidel, A.; Scheffler, R.; Gowda, S.; Luntz, A. C. *J. Phys. Chem. Lett.* **2013**, *4*, 556−560.
(4) Jiang, R.; Tran, D. T.; McClure, J. P.; Chu, D. *ACS Catal.* **2014**, *4*, 2577−2586.
(5) Saveant, J. M. *Annual review of analytical chemistry* **2014**, *7*, 537−560.
(6) Karlberg, G. S.; Jaramillo, T. F.; Skulason, E.; Rossmeisl, J.; Bligaard, T.; Norskov, J. K. *Phys. Rev. Lett.* **2007**, *99*, 126101.
(7) Tafel, J. *Z. Phys. Chem.* **1905**, *50*, 641−712.
(8) Holewinski, A.; Linic, S. *J. Electrochem. Soc.* **2012**, *159*, H864−H870.
(9) Wu, J. B.; Zhang, J. L.; Peng, Z. M.; Yang, S. C.; Wagner, F. T.; Yang, H. *J. Am. Chem. Soc.* **2010**, *132*, 4984−4985.
(10) Yan, Y.; Xia, B.; Xu, Z.; Wang, X. *ACS Catal.* **2014**, *4*, 1693−1705.
(11) Surendranath, Y.; Kanan, M. W.; Nocera, D. G. *J. Am. Chem. Soc.* **2010**, *132*, 16501−16509.
(12) Kanan, M. W.; Nocera, D. G. *Science* **2008**, *321*, 1072−1075.
(13) Shi, Z.; Liu, M.; Atrens, A. *Corros. Sci.* **2010**, *52*, 579−588.
(14) Rosborg, B.; Pan, J. S.; Leygraf, C. *Corros. Sci.* **2005**, *47*, 3267−3279.
(15) Suntivich, J.; May, K. J.; Gasteiger, H. A.; Goodenough, J. B.; Shao-Horn, Y. *Science* **2011**, *334*, 1383−1385.
(16) Domenech, A.; Teresa Domenech-Carbo, M.; Pasies, T.; Carmen Bouzas, M. *Electroanalysis* **2011**, *23*, 2803−2812.
(17) Domenech, A.; Domenech-Carbo, M. T.; Edwards, H. G. M. *Anal. Chem.* **2008**, *80*, 2704−2716.
(18) Bediako, D. K.; Surendranath, Y.; Nocera, D. G. *J. Am. Chem. Soc.* **2013**, *135*, 3662−3674.
(19) Macounova, K.; Jirkovsky, J.; Makarova, M. V.; Franc, J.; Krtil, P. *J. Solid State Electrochem.* **2009**, *13*, 959−965.
(20) Guerrini, E.; Trasatti, S. *Russ. J. Electrochem.* **2006**, *42*, 1017−1025.

(21) Bard, A. J.; Faulkner, L. R. *Electrochemical Methods: Fundamentals and Applications*, 2nd ed.; John Wiley & Sons, Inc.: New York. 2001.
(22) Schmickler, W. *Annu. Rep. Prog. Chem., Sect. C: Phys. Chem.* **1999**, *95*, 117−162.
(23) Ignaczak, A.; Schmickler, W. *Electrochim. Acta* **2007**, *52*, 5621−5633.
(24) Grimminger, J.; Schmickler, W. *Chem. Phys.* **2007**, *334*, 8−17.
(25) Schmickler, W. *Chem. Rev.* **1996**, *96*, 3177−3200.
(26) Mohr, J.-H.; Schmickler, W. *Phys. Rev. Lett.* **2000**, *84*, 1051−1054.
(27) Damjanov, A.; Dey, A.; Bockris, J. O. M. *Electrochim. Acta* **1966**, *11*, 791−814.
(28) Da Silva, L. M.; Boodts, J. F. C.; De Faria, L. A. *Electrochim. Acta* **2001**, *46*, 1369−1375.
(29) Chen, S.; Ferreira, P. J.; Sheng, W. C.; Yabuuchi, N.; Allard, L. F.; Shao-Horn, Y. *J. Am. Chem. Soc.* **2008**, *130*, 13818−13819.
(30) Anderson, A. B.; Albu, T. V. *J. Am. Chem. Soc.* **1999**, *121*, 11855−11863.
(31) Taylor, C. D.; Wasileski, S. A.; Filhol, J. S.; Neurock, M. *Phys. Rev. B* **2006**, *73*, 165402.
(32) Bonnet, N.; Morishita, T.; Sugino, O.; Otani, M. *Phys. Rev. Lett.* **2012**, *109*, 266101.
(33) Jinnouchi, R.; Anderson, A. B. *Phys. Rev. B* **2008**, *77*, 245417.
(34) Rossmeisl, J.; Logadottir, A.; Norskov, J. K. *Chem. Phys.* **2005**, *319*, 178−184.
(35) Gouy, G. *J. Phys. Theor. Appl.* **1910**, *9*, 457−468.
(36) Chapman, D. L. *Philos. Mag.* **1913**, *25*, 475−481.
(37) Stern, O. *Z. Elektrochem. Angew. Phys. Chem.* **1924**, *30*, 508−516.
(38) Anderson, A. B.; Cai, Y. *J. Phys. Chem. B* **2004**, *108*, 19917−19920.
(39) Filhol, J. S.; Neurock, M. *Angew. Chem., Int. Ed.* **2006**, *45*, 402−406.
(40) Skulason, E.; Karlberg, G. S.; Rossmeisl, J.; Bligaard, T.; Greeley, J.; Jonsson, H.; Norskov, J. K. *Phys. Chem. Chem. Phys.* **2007**, *9*, 3241−3250.
(41) Santana, J. A.; Mateo, J. J.; Ishikawa, Y. *J. Phys. Chem. C* **2010**, *114*, 4995−5002.
(42) Fang, Y. H.; Liu, Z. P. *J. Am. Chem. Soc.* **2010**, *132*, 18214−18222.
(43) Fang, Y.-H.; Wei, G.-F.; Liu, Z.-P. *J. Phys. Chem. C* **2014**, *118*, 3629−3635.
(44) Fang, Y. H.; Wei, G. F.; Liu, Z. P. *Catal. Today* **2013**, *202*, 98−104.
(45) Fang, Y.-H.; Wei, G.-F.; Liu, Z.-P. *J. Phys. Chem. C* **2013**, *117*, 7669−7680.
(46) Wei, G.-F.; Fang, Y.-H.; Liu, Z.-P. *J. Phys. Chem. C* **2012**, *116*, 12696−12705.
(47) Klaus, M. *J. Res. Inst. Catal., Hokkaido Univ.* **1969**, *17*, 54−75.
(48) Burstein, G. T. *Corros. Sci.* **2005**, *47*, 2858−2870.
(49) Castelli, P.; Trasatti, S.; Pollak, F. H.; Ogrady, W. E. *J. Electroanal. Chem.* **1986**, *210*, 189−194.
(50) Gomez, R.; Fernandez-Vega, A.; Feliu, J.; Aldaz, A. *J. Phys. Chem.* **1993**, *97*, 4769−4776.
(51) Markovic, N. M.; Grgur, B. N.; Ross, P. N. *J. Phys. Chem. B* **1997**, *101*, 5405−5413.
(52) Housmans, T.; Koper, M. *J. Phys. Chem. B* **2003**, *107*, 8557−8567.
(53) Lu, G.-Q.; Chrzanowski, W.; Wieckowski, A. *J. Phys. Chem. B* **2000**, *104*, 5566−5572.
(54) Liu, S. X.; Liao, L. W.; Tao, Q.; Chen, Y. X.; Ye, S. *Phys. Chem. Chem. Phys.* **2011**, *13*, 9725−9735.
(55) Weaver, M. J.; Anson, F. C. *J. Phys. Chem.* **1976**, *80*, 1861−1866.
(56) Saveant, J. M.; Tessier, D. *J. Phys. Chem.* **1977**, *81*, 192−2197.
(57) Liu, H. Y.; Hupp, J. T.; Weaver, M. J. *J. Electroanal. Chem.* **1984**, *179*, 219−238.
(58) Hupp, J. T.; Liu, H. Y.; Farmer, J. K.; Gennett, T.; Weaver, M. J. *J. Electroanal. Chem.* **1984**, *168*, 313−334.
(59) Antonello, S.; Maran, F. *J. Am. Chem. Soc.* **1999**, *121*, 9668−9676.
(60) Antonello, S.; Formaggio, F.; Moretto, A.; Toniolo, C.; Maran, F. *J. Am. Chem. Soc.* **2001**, *123*, 9577−9584.
(61) Saveant, J.; Tessier, D. *J. Phys. Chem.* **1978**, *82*, 1723−1727.
(62) Fletcher, S.; Varley, T. S. *Phys. Chem. Chem. Phys.* **2011**, *13*, 5359−5364.
(63) Fletcher, S. *J. Solid State Electrochem.* **2009**, *13*, 537−549.
(64) Petrii, O. A.; Nazmutdinov, R. R.; Bronshtein, M. D.; Tsirlina, G. A. *Electrochim. Acta* **2007**, *52*, 3493−3504.
(65) Gileadi, E.; Kirowa-Eisner, E. *Corros. Sci.* **2005**, *47*, 3068−3085.
(66) Björketun, M. E.; Tripkovic, V.; Skúlason, E.; Rossmeisl, J. *Catal. Today* **2013**, *202*, 168−174.
(67) German, E.; Kuznetsov, A. *J. Phys. Chem.* **1994**, *98*, 6120−6127.
(68) Saveant, J. M. *J. Am. Chem. Soc.* **1987**, *109*, 6788−6795.
(69) Nazmutdinov, R. R.; Glukhov, D. V.; Tsirlina, G. A.; Petrii, O. A. *Russ. J. Electrochem.* **2002**, *38*, 720−731.
(70) Gutman, E. M. *Corros. Sci.* **2005**, *47*, 3086−3096.
(71) Santos, E.; Schmickler, W. *Chem. Phys.* **2007**, *332*, 39−47.
(72) Schmickler, W. *Chem. Phys. Lett.* **2000**, *317*, 458−463.
(73) Ignaczak, A.; Schmickler, W. *Chem. Phys.* **2002**, *278*, 147−158.
(74) Liu, Y.; Wang, L. W.; Wang, G.; Deng, C.; Wu, B.; Gao, Y. *J. Phys. Chem. C* **2010**, *114*, 21417−21422.
(75) Bockris, J. O. M.; Koch, D. F. A. *J. Phys. Chem.* **1961**, *65*, 1941−1948.
(76) Wang, J. X.; Springer, T. E.; Adzic, R. R. *J. Electrochem. Soc.* **2006**, *153*, A1732−A1740.
(77) Strmcnik, D.; Tripkovic, D.; van der Vliet, D.; Stamenkovic, V.; Markovic, N. M. *Electrochem. Commun.* **2008**, *10*, 1602−1605.
(78) Skulason, E.; Tripkovie, V.; Bjorketun, M. E.; Gudmundsdottir, S.; Karlberg, G.; Rossmeisl, J.; Bligaard, T.; Jonsson, H.; Norskov, J. K. *J. Phys. Chem. C* **2010**, *114*, 18182−18197.
(79) Yang, F.; Zhang, Q. F.; Liu, Y. W.; Chen, S. L. *J. Phys. Chem. C* **2011**, *115*, 19311−19319.
(80) Liu, S. X.; Liao, L. W.; Tao, Q.; Chen, Y. X.; Ye, S. *Phys. Chem. Chem. Phys.* **2011**, *13*, 9725−9735.
(81) Wang, H. F.; Liu, Z. P. *J. Phys. Chem. C* **2009**, *113*, 17502−17508.
(82) Gao, W.; Keith, J. A.; Anton, J.; Jacob, T. *J. Am. Chem. Soc.* **2010**, *132*, 18377−18385.
(83) Beni, G.; Schiavone, L. M.; Shay, J. L.; Dautremontsmith, W. C.; Schneider, B. S. *Nature* **1979**, *282*, 281−283.
(84) Bockris, J. O. M. *Int. J. Hydrogen Energy* **1999**, *24*, 1−15.
(85) Trasatti, S. *Electrochim. Acta* **1984**, *29*, 1503−1512.
(86) Marshall, A. T.; Sunde, S.; Tsypkin, A.; Tunold, R. *Int. J. Hydrogen Energy* **2007**, *32*, 2320−2324.
(87) Koper, M. T. M.; van Santen, R. A. *J. Electroanal. Chem.* **1999**, *476*, 64−70.
(88) Patrito, E. M.; Paredes-Olivera, P. *Surf. Sci.* **2003**, *527*, 149−162.
(89) Hyman, M. P.; Medlin, J. W. *J. Phys. Chem. B* **2005**, *109*, 6304−6310.
(90) Panchenko, A.; Koper, M. T. M.; Shubina, T. E.; Mitchell, S. J.; Roduner, E. *J. Electrochem. Soc.* **2004**, *151*, A2016−A2027.
(91) Karlberg, G. S.; Rossmeisl, J.; Norskov, J. K. *Phys. Chem. Chem. Phys.* **2007**, *9*, 5158−5161.
(92) Lozovoi, A. Y.; Alavi, A. *Phys. Rev. B* **2003**, *68*, 245416.
(93) Lozovoi, A. Y.; Alavi, A.; Kohanoff, J.; Lynden-Bell, R. M. *J. Chem. Phys.* **2001**, *115*, 1661−1669.
(94) Sha, Y.; Yu, T. H.; Merinov, B. V.; Goddard, W. A., III *ACS Catal.* **2014**, *4*, 1189−1197.
(95) Sha, Y.; Yu, T. H.; Merinov, B. V.; Shirvanian, P.; Goddard, W. A., III *J. Phys. Chem. C* **2012**, *116*, 21334−21342.
(96) Sheng, T.; Lin, W. F.; Hardacre, C.; Hu, P. *Phys. Chem. Chem. Phys.* **2014**, *16*, 13248−13254.
(97) Groß, A.; Gossenberger, F.; Lin, X.; Naderian, M.; Sakong, S.; Roman, T. *J. Electrochem. Soc.* **2014**, *161*, E3015−E3020.
(98) Filhol, J. S.; Doublet, M. L. *Catal. Today* **2013**, *202*, 87−97.

(99) Gunceler, D.; Letchworth-Weaver, K.; Sundararaman, R.; Schwarz, K. A.; Arias, T. A. *Modelling Simul. Mater. Sci. Eng.* **2013**, *21*, 074005.
(100) Hamada, I.; Sugino, O.; Bonnet, N.; Otani, M. *Phys. Rev. B* **2013**, *88*, 155427.
(101) Zhang, T.; Anderson, A. B. *J. Phys. Chem. C* **2009**, *113*, 3197−3202.
(102) Zhang, T.; Anderson, A. B. *Electrochim. Acta* **2007**, *53*, 982−989.
(103) Anderson, A. B.; Neshev, N. M.; Sidik, R. A.; Shiller, P. *Electrochim. Acta* **2002**, *47*, 2999−3008.
(104) Sidik, R. A.; Anderson, A. B. *J. Electroanal. Chem.* **2002**, *528*, 69−76.
(105) Anderson, A. B.; Neshev, N. M. *J. Electrochem. Soc.* **2002**, *149*, E383−E388.
(106) Cai, Y.; Anderson, A. B. *J. Phys. Chem. B* **2004**, *108*, 9829−9833.
(107) Gomer, R.; Tryson, G. *J. Chem. Phys.* **1977**, *66*, 4413−4424.
(108) Reiss, H.; Heller, A. *J. Phys. Chem.* **1985**, *89*, 4207−4213.
(109) Rostamikia, G.; Janik, M. J. *J. Electrochem. Soc.* **2009**, *156*, B86−B92.
(110) Taylor, C. D.; Neurock, M. *Curr. Opin. Solid State Mater. Sci.* **2005**, *9*, 49−65.
(111) Taylor, C.; Kelly, R. G.; Neurock, M. *J. Electrochem. Soc.* **2006**, *153*, E207−E214.
(112) Janik, M. J.; Taylor, C. D.; Neurock, M. *Top. Catal.* **2007**, *46*, 306−319.
(113) Taylor, C.; Kelly, R. G.; Neurock, M. *J. Electrochem. Soc.* **2007**, *154*, F55−F64.
(114) Cao, D.; Lu, G. Q.; Wieckowski, A.; Wasileski, S. A.; Neurock, M. *J. Phys. Chem. B* **2005**, *109*, 11622−11633.
(115) Mamatkulov, M.; Filhol, J. S. *Phys. Chem. Chem. Phys.* **2011**, *13*, 7675−7684.
(116) Janik, M. J.; Neurock, M. *Electrochim. Acta* **2007**, *52*, 5517−5528.
(117) Taylor, C. D.; Kelly, R. G.; Neurock, M. *J. Electroanal. Chem.* **2007**, *607*, 167−174.
(118) Rossmeisl, J.; Norskov, J. K.; Taylor, C. D.; Janik, M. J.; Neurock, M. *J. Phys. Chem. B* **2006**, *110*, 21833−21839.
(119) Kilic, M. S.; Bazant, M. Z.; Ajdari, A. *Phys. Rev. E* **2007**, *75*, 021502.
(120) Borukhov, I.; Andelman, D.; Orland, H. *Phys. Rev. Lett.* **1997**, *79*, 435−438.
(121) Andreussi, O.; Dabo, I.; Marzari, N. *J. Chem. Phys.* **2012**, *136*, 064102.
(122) Fornberg, B.; Sloan, D. M. *Acta Numerica* **1994**, *3*, 203−267.
(123) Fattebert, J. L.; Gygi, F. *J. Comput. Chem.* **2002**, *23*, 662−666.
(124) Shang, C.; Liu, Z.-P. *J. Am. Chem. Soc.* **2011**, *133*, 9938−9947.
(125) Li, Y.-F.; Liu, Z.-P.; Liu, L.-L.; Gao, W.-G. *J. Am. Chem. Soc.* **2010**, *132*, 13008−13015.
(126) Björketun, M. E.; Zeng, Z. H.; Ahmed, R.; Tripkovic, V.; Thygesen, K. S.; Rossmeisl, J. *Chem. Phys. Lett.* **2013**, *555*, 145−148.
(127) Fang, Y. H.; Liu, Z. P. *J. Phys. Chem. C* **2009**, *113*, 9765−9772.
(128) Fang, Y. H.; Liu, Z. P. *J. Phys. Chem. C* **2010**, *114*, 4057−4062.
(129) Cuesta, A. *Surf. Sci.* **2004**, *572*, 11−22.
(130) Hoshi, N.; Asaumi, Y.; Nakamura, M.; Mikita, K.; Kajiwara, R. *J. Phys. Chem. C* **2009**, *113*, 16843−16846.
(131) Fang, Y.-H.; Liu, Z.-P. *Surf. Sci.* **2014**, DOI: 10.1016/j.susc.2014.05.014.